CLM-P840

CLM-P840

Large scale mixing simulations using CHYMES

D. F. Fletcher

UK ATOMIC ENERGY AUTHORITY

Culham Laboratory

CLM-P840

Large scale mixing simulations using CHYMES

D.F. Fletcher

Culham Laboratory, Abingdon, Oxon., OX14 3DB

ABSTRACT

In this paper we report on further developments to the Culham multiphase mixing code (CHYMES). These modifications include a more realistic geometrical representation of hemispherically shaped vessels, a simple model of melt pools or particulate beds and different fragmentation modelling. Results are presented which illustrate the capability of the code, as well as some conclusions from a simple parameter variation study. In the final section we discuss the current state of validation of the model and make some suggestions for future work.

(Submitted for publication in Nuclear Science and Engineering)

June, 1988

Contents

1 Introduction

If a hot liquid is poured into a cooler volatile liquid, in some circumstances the cold liquid can be vaporised so quickly that an explosion results. Such explosions are known variously as vapour explosions, Molten Fuel Coolant Interactions (MFCIs) and steam explosions [1]. They are studied in the nuclear industry, since in the unlikely event that the core melts and pours into residual coolant such an explosion may result, causing severe damage to the reactor and possibly failure of the reactor containment. In particular, in the case of Light Water Reactors this hypothetical event is termed an alpha-mode failure and has been the subject of a number of probabilistic studies [2,3,4]. At Culham Laboratory an improved study is underway, in which discrete models of the mixing, triggering, propagation and expansion phases of the explosion are being combined to determine the probability of alpha-mode failure [5]. In this paper we concentrate on results from the new mixing model developed as part of this study.

The coarse mixing stage of a vapour explosion has been studied theoretically at Culham Laboratory for approximately 4 years. This work started with a review of the available models [6] which identified the need to develop a more sophisticated 3-component (melt, water and steam) multiphase flow model. Such a model has been under development for approximately 3 years. This model, called CHYMES, has formed the basis of a number of theoretical studies of coarse mixing [7,8,9,10,11]. Most recently it has been used to perform large scale simulations as part of an international comparison exercise [12]. In addition, a compressible flow version of the code has been developed [13]. Calculations reported in reference 13 show that allowing for compressibility does not affect the solution significantly but decreases the run time of the code by a factor of approximately two.

In this paper we report on some further developments and modifications to the code which improve its usefulness in reactor safety studies. These include a better representation of complex geometries, a simple model of melt pools or particulate beds and alternative fragmentation modelling. The paper is organised as follows: in section 2 the new features of the code are described. In section 3 we present results from some new simulations and a limited parameter survey. In section 4 we present our conclusions and some suggestion for future modifications to CHYMES.

2 Description of the New Features

In this section we will describe recent modification to the CHYMES code. Before describing these changes a brief summary of the current state of the CHYMES model will be given. We use the standard equations of multiphase flow to model the transient flow of three species (melt, water and steam) in a two-dimensional (axisymmetric) geometry. The presence of each species is specified using a volume fraction and each species has its own velocity field. In addition, equations can be solved to determine the melt temperature and the melt and/or water length-scales. The melt is assumed to be incompressible and the water and steam have barotropic equations of state (i.e. the pressure is a function of the density only). The steam is always assumed to be at its saturation temperature and the water is assumed to remain at its initial temperature. At present condensation is not modelled. For completeness we give some sample equa-

tions below. A full description of the conservation equations, the constitutive relations and the solution procedure used can be found in references 8, 9 and 13. To illustrate the types of equations being solved we will present the equations for conservation of mass and momentum for the water phase. Conservation of water mass gives:

$$\frac{\partial}{\partial t}(\alpha_w \rho_w) + \frac{1}{r}\frac{\partial}{\partial r}(r\alpha_w \rho_w U_w) + \frac{\partial}{\partial z}(\alpha_w \rho_w V_w) = -\dot{m}_w \tag{1}$$

and conservation of momentum in the radial and axial directions gives:

$$\frac{\partial}{\partial t}(\alpha_w \rho_w U_w) + \frac{1}{r}\frac{\partial}{\partial r}(r\alpha_w \rho_w U_w^2) + \frac{\partial}{\partial z}(\alpha_w \rho_w U_w V_w) =$$
$$-\alpha_w \frac{\partial p}{\partial r} + K_{sw}^r(U_s - U_w) + K_{mw}^r(U_m - U_w) + F_{\dot{m}w}^r \tag{2}$$

and

$$\frac{\partial}{\partial t}(\alpha_w \rho_w V_w) + \frac{1}{r}\frac{\partial}{\partial r}(r\alpha_w \rho_w U_w V_w) + \frac{\partial}{\partial z}(\alpha_w \rho_w V_w^2) =$$
$$-\alpha_w \frac{\partial p}{\partial z} - g\alpha_w \rho_w + K_{sw}^z(V_s - V_w) + K_{mw}^z(V_m - V_w) + F_{\dot{m}w}^z \ . \tag{3}$$

In the above equations α is the volume fraction, ρ is the density, U, V are the radial and axial velocities, g is the acceleration due to gravity, p is the pressure, t is time and r, z are the radial and axial coordinates. The term $-\dot{m}_w$ is the water mass loss rate due to evaporation and the K_{sw}^r etc. are momentum exchange coefficients. The terms on the RHS of the momentum equations model the effect of the pressure gradient force, the buoyancy force due to gravity, inter-component drag and the evaporation reaction force.

In addition to the above equations we also have the constraint

$$\alpha_w + \alpha_m + \alpha_s = 1 \tag{4}$$

and a number of additional equations of the same form as equation (1) to model the change in melt and water length-scales and the melt temperature.

2.1 Complex Geometries

The modifications to the code to allow simple regions to be blanked out were described in reference 12. The code uses a uniform finite difference mesh and the user is allowed to blank out any regions which correspond to grid cells. At the boundary of these regions the normal velocity of each species is automatically set to zero in the code. The main modifications required to allow more sophisticated geometries to be modelled was to make the contour plotting packages more general, so that arbitrary regions could be blanked out. The resulting plotting packages are run on a workstation (a Whitechapel MG-200) after the data has been produced on the CRAY-2. They allow the user to plot volume fractions, velocity vectors, length-scales, the melt temperature or the Θ – function (an empirical mixing index [10]).

Figure 1(a) shows the geometry used in earlier large scale mixing calculations (and chosen for the international test case [12]). Figure 1(b) shows a representation of a hemispherically based vessel using a finite difference grid with 22 cells in the radial

direction and 20 cells in the vertical direction. Even though the grid is relatively coarse it provides a good representation of a vessel with a hemispherical base. The large horizontal surfaces which caused melt to collect in earlier calculations are seen to be absent.

2.2 Melt Pool Model

In large scale mixing simulations there is a tendency for melt to form a pool in the bottom of the vessel. If a cell is completely filled with melt (i.e. $\alpha_m = 1$) there is no way to determine the pressure in that cell, since the melt is assumed to be incompressible. To avoid this problem and to provide a means of modelling solid debris, an option has been included in the code to stop solving in a particular cell if the melt volume fraction exceeds a critical value. For molten material a value of α_{crit} of 0.98 has been used in the simulations reported in this paper. The normal velocities of *all* the species are set to zero when this condition is satisfied. For solid debris a value of 0.6, corresponding to dense packing of particles, say, could be used. In this case only the melt velocity needs to be set to zero, as the water/steam can continue to flow into the cell and the pressure can be obtained from the EOS of the water/steam mixture. The melt enthalpy equation can be used to determine whether the melt is in solid or liquid form.

It should be noted that this model is very simple and there is no model of reagglomeration of melt particles i.e. the melt length-scale is not increased in a pool. Also this model does not remove the problem of artificial mixing caused by poor resolution of the real flow. For example, a cell containing 50% melt and 50% water would suggest that the melt and water were well mixed. However, if the cell size were halved this cell would be split into two cells with perhaps the bottom cell filled with melt and the top cell filled with water, suggesting that there was no mixing. There is no way around this fundamental problem if a standard Eulerian multiphase flow formulation is used. It is up to the user to choose a fine enough grid to ensure that any melt pools are adequately resolved.

2.3 Melt Fragmentation Model

Results obtained using a parametric melt fragmentation model, where the final particle size and the fragmentation rate were user-specified constants, were reported in an earlier paper [9]. In this section we describe the implementation of an alternative fragmentation model developed at Sandia National Laboratory [14]. In Lagrangian coordinates the fragmentation rate is determined from:

$$\frac{DL_m}{Dt} = -C_0 |V_{rel}| \sqrt{\frac{\rho_f}{\rho_m}}. \tag{5}$$

In equation (5), L_m is the melt length-scale, $V_{rel} = (V_f - V_m)$ is the velocity difference between the melt and the steam-water mixture, ρ_m is the melt density and ρ_f is the fluid density. The fluid density and velocity are defined as

$$\rho_f = \frac{\rho_w \alpha_w + \rho_s \alpha_s}{\alpha_w + \alpha_s} \tag{6}$$

and

$$V_f = \frac{V_w \rho_w \alpha_w + V_s \rho_s \alpha_s}{\rho_w \alpha_w + \rho_s \alpha_s} \tag{7}$$

respectively. Thus the fluid causing breakup of the melt is assumed to have the mass averaged properties of those of the steam and water. The empirical constant C_0 takes a value of 0.245 [14]. Equation (5) is easily converted to Eulerian conservation form by multiplying both sides of the equation by $\rho_m \alpha_m$ and using the continuity equation for the melt to bring the $\rho_m \alpha_m$ factor inside the derivative.

The above model allows the particles to breakup until their velocity is equilibrated with the surrounding fluid. Because the RHS of equation (5) is not proportional to the current length-scale the equation does not guarantee a positive length-scale. Physically this means that the breakup rate does not depend directly on the current particle size. In CHYMES the user can specify a minimum particle size (a value of 1mm is usually used) to prevent the particles becoming too small.[1] In addition, in the calculation reported in this paper the Weber number was evaluated in each cell at the beginning of each time-step and fragmentation was not allowed during that time-step if the Weber number was less than 12. It is very easy to modify this practice, if desired, to allow the fragmentation rate and final particle size to depend on any of the flow variables.

This model has also been used to determine the water length-scale. In this case it is assumed that the water is in droplet form surrounded by flowing steam, so that $\rho_f = \rho_s$ and $V_f = V_s$. The implementation of this model is exactly the same as that for the melt species (with the slight complication that the RHS of the water mass conservation equation is non zero). Results obtained using this model are given in section 3.2.

3 Results from the Simulations

We now present the results from some large scale mixing simulations performed with the CHYMES code. In section 3.1 we present some calculations carried out for the geometry shown in figure 1(a). These investigate the effect of some uncertain modelling parameters. In section 3.2 we present results obtained for the modified geometry, shown in figure 1(b). These also demonstrate the effect of the fragmentation models described in section 2.3.

3.1 Parameter Survey

In this section we present the results of a series of calculations carried out to investigate the importance of various parameters and models. The geometry and initial conditions, shown in figure 1(a), were the same as those used in the earlier large scale simulations [12]. The melt was assumed to pour into the vessel through a perforated plate for the duration of the calculation (1.5s). A finite difference grid with 11 radial and 10 axial cells was used (except in the grid refinement study). A time-step of $20\mu s$ was used. Table 1 gives a description of the computations performed. In all cases the general drag law proposed by Harlow and Amsden [15] was used. In the base case calculation

[1] In previous calculations we set the RHS of equation (5) to $-(L_m - L_{crit})/\tau_{frag}$ where L_{crit} was a user-specified minimum size and τ_{frag} was a user-specified fragmentation rate, where both L_{crit} and τ_{frag} could be functions of any local variables [9].

Calc.	Description	Purpose
1	Base case	Compressible version of international test case [12]
2	Water & steam length = 5mm	Small length-scales
3	Water & steam length = 100mm	Large length-scales
4	$C_D = 0.6$	High drag coefficient
5	$C_D = 0.06$	Low drag coefficient
6	$\alpha_s(t = 0) = 0.005$	Effect of vapour in pool
7	Modified heat transfer model	Lower bound model [16]
8	Fine grid	Check grid independence

Table 1: Description of Calculations

all the drag coefficients were set to 0.2 and all the length-scales to 20mm. The melt length-scale (20mm) and temperature (2500K) were kept fixed as these parameters are known to affect mixing significantly [7,8].

Calculation 1 provides a base case. Results from this simulation have been compared with the results from an incompressible flow simulation in reference 13. Calculations 2–5 were performed to examine the effect of the magnitude of the inter-component drag. Calculation 6 was for a situation where there was virtually no vapour in the the water pool initially (0.5% instead of 5% in the base case). A lower bound heat transfer model was used in calculation 7. In this calculation the radiation heat flux was multiplied by a factor of 0.8 to account for incomplete absorption of radiation in a reasonable depth of water (see reference 16 for details). Also the standard convective film boiling correlation of Witte [17] was replaced by an ad hoc lower bound vapour film conduction model. The film boiling heat transfer coefficient was set equal to

$$h = \frac{k}{\delta} \tag{8}$$

where k is the vapour thermal conductivity and δ is a vapour film thickness, obtained by assuming that *all* the vapour surrounds the melt particles. It is fully described in reference 16. Finally, calculation 8 was for a finite difference grid with twice as many grid points in each direction and the time-step reduced by a factor of four.

3.1.1 Sweep-out

Table 2 shows the mass of each species expelled from the vessel after 1.5s. The data given in Table 2 shows that changing the drag changes the melt sweep-out significantly. Thus accurately measured melt sweep-out data from experiments provides good data with which to test the drag modelling. The water and steam sweep-out is affected less by changes to the drag since the water/steam mixture has to be expelled to make space for the inflowing melt (since water is virtually incompressible under these conditions). Reducing the initial vapour fraction in the melt pool has little effect, other than to increase the mass of water which can be swept-out. Changing the heat transfer model reduces the vapour production rate and consequently reduces the sweep-out. Comparison of the results for the coarse (calculation 1) and the fine (calculation 8) grids shows that the sweep-out is virtually unaffected.

Calc.	Melt expelled (tonnes)	Water expelled (tonnes)	Steam expelled (tonnes)
1	0.62	15.67	0.20
2	5.73	16.11	0.16
3	0.06	13.58	0.22
4	3.53	16.16	0.18
5	0.04	13.90	0.20
6	0.59	16.54	0.20
7	0.30	14.84	0.16
8	0.59	15.01	0.19

Table 2: Mass of each species expelled after 1.5s

Examination of the transient sweep-out data shows that in the different simulations the behaviour is qualitatively very similar to that given in reference 12, with the exception of the high melt sweep-out for calculations 2 and 4 and the very low sweep-out for calculations 3 and 5.

3.1.2 The Transient Steaming Rate

The transient steaming rate for the different simulations is shown in figure 2. The most striking thing about the figure is the similarity of all the cases. It would be virtually impossible to distinguish between the different cases experimentally. As expected the modified heat transfer model leads to the lowest steaming rate and the low drag simulations to the highest (since more melt and water are retained in the vessel). At late times the fine grid solution shows a slight reduction in the steaming rate compared with the coarse grid solution due to the settling out of melt to form a pool, as described in section 2.2. At the end of the calculation 26 cells were filled with melt. Melt pools were located both in the central well of the vessel and on the two lower horizontal steps.

Figure 3 shows the transient pressurization of the vessel for calculation 1. This plot is typical of those obtained from the simulations. The pressure rises initially as melt pours into the vessel and compresses the water/steam mixture. As flows develop material is expelled through the vent and the pressure falls. The figure shows that there is indeed very little pressurization of the vessel during mixing.

3.1.3 Measures of Mixing

We have compared the mixing in the different cases using two different measures. Figure 4 shows the mass of melt mixed using an empirical method developed by Theofanous [18]. Melt is considered to be mixed if the coolant surrounding the melt has a void fraction less than a certain value (a value of 70% was used here). The figure shows that the mass mixed in this situation is virtually identical for all except the high drag calculations (2 and 4). In most of the calculations the melt mass mixed increased monotonically to a value of around 25 tonnes. In the fine grid simulation the mass mixed starts to fall after about 1.3s as the melt separates out from the remaining water.

Calc.	Description	Purpose
9	Modified Geometry	Removal of horizontal surfaces
10	Melt fragmentation	Test Sandia fragmentation model
11	Melt and water fragmentation	Effect of variable water length-scale

Table 3: Description of Improved Modelling Calculations

The second method uses the Θ–function described in references 8 and 10. Since the melt length-scale is kept fixed in the present simulations *no* allowance for the effect of particle size was made. Figure 5 shows the mass of melt where $\theta < 0.5$ as a function of time. Again the results are very similar in most cases with the mass of melt mixed increasing with time to a value of around 10 tonnes. As discussed in reference 12 most of the mixing which occurs at late times is due to the accumulation of melt and water on horizontal surfaces, and is therefore an artifact of the chosen geometry. This will be explicitly demonstrated in the next section when we present results obtained using the modified geometry.

The most interesting feature of these simulations is the insensitivity of the outcome to the modelling changes made. In particular, the mass of melt mixed is more sensitive to the chosen criterion (e.g. the critical value of θ) than it is to most of the modelling assumptions.

3.2 Improved Modelling

In this section we present the results from three simulations using the modified geometry shown in Figure 1(b). The calculations are summarised in Table 3. Calculation 9 examines the effect of the improved geometry and calculations 10 and 11 test fragmentation models for the melt and water droplets. A limited number of test cases were performed as these simulations are relatively expensive (~8500s on a CRAY-2).

3.2.1 Sweep-out

The transient melt and water sweep-out data for the three different simulations is shown in Figure 6. The main difference between the three different cases is the melt mass lost. This is negligible in the fixed length-scale case but significant in the other two cases. This is because melt fragmentation reduces the particle size and thus the drag on the particles is increased. When water fragmentation is modelled less melt is swept-out. This is because the water particle size falls in regions where there are large steam velocities and the water is rapidly swept-out of these regions. Consequently, less steam is produced and the drag on the melt is reduced (c.f. steaming rate data discussed in the next subsection).

Figure 7 shows the average fragment sizes as a function of time for the two simulations with melt fragmentation. The data shows that the *average* melt particle size is of the order of 5mm. This is consistent with experimental data from intermediate scale experiments [19,20]. Note that the average melt particle size can rise with time as melt is being injected into the vessel, whereas the water length-scale must always decrease.

The water length-scale decreases very rapidly to the preset minimum of 2mm. There is less fragmentation of the melt in this case because of the effect described above.

3.2.2 The Transient Steaming Rate

Figure 8 shows the transient steaming rate for the three different cases. The figure shows that in the case when only melt fragmentation was modeled there is a large spike at around 0.6s, corresponding to the minimum average melt particle size. This caused the pressure in the vessel to rise transiently to 5bars. There was another smaller spike after about 1.1s which caused the pressure to rise to about 2.5bars. When water fragmentation is modelled this behaviour is absent, due to the effect described in subsection 3.2.1 above, and the steaming rate and pressure change is qualitatively very similar to that for the case without fragmentation.

These results suggest that it is very important to model all features of the problem correctly. If melt fragmentation alone is modelled the melt particles break-up, the steaming rate rises but water cannot be expelled from the mixture fast enough to lower the steaming rate. This does not mean that the results from the simulation with melt fragmentation only are wrong (since the fragmentation models have not been fully validated) but it does illustrate the complex nature of the problem and the need for careful experimental validation of the complete model.

3.2.3 Measures of Mixing

Figure 9 shows the mass of melt mixed according to the criterion developed by Theofanous [18]. The figure shows that allowing for fragmentation reduces the mass of melt mixed considerably. In addition, the data given in the figure shows that improving the geometrical representation leads to more mixing for this index of mixing.

Figure 10 shows the mass of melt where $\theta > 0.5$ as a function of time. In this case there is less mixing when the improved geometrical representation is used. Allowing for melt fragmentation reduces the mixing significantly. The mixing is improved when water fragmentation is added, with a period of approximately 0.3s duration around 1.3s when there is a peak in the mass of melt mixed. This occurs when the melt and remaining water settle on the base of the vessel.

Figures 11(a), (b) and (c) show the contour plot of θ at a time of 0.45s. The dispersive effect of allowing for melt fragmentation is clearly illustrated. Figures 12(a), (b) and (c) show the contour plots at a later time of 0.8s. There is virtually no mixing in the case when melt fragmentation alone is modelled. In the other two cases the lower half of the vessel contains some mixture. Finally, figures 13(a), (b) and (c) show the contour plots after 1.4s. In the case with no fragmentation a large melt pool has formed with a region of mixture on top of it. In the second case there is a small melt pool with some mixing above it and in the third case there is no melt pool and some poor mixing around the edge of the vessel. These plots illustrate the tendency for mixture to form on top of melt pools. However, it should be remembered that the present model does not simulate this situation, of water separated from the melt by a layer of steam, as a statified system as observed in experiments [21].

4 Conclusions and Future Work

In this paper we have presented a summary of the status of the development of the coarse mixing code CHYMES. In addition, a number of new developments have been described. These include an improved representation of the geometry of hemispherical mixing vessels, a simple model of melt pool formation and fragmentation models for the melt and water species.

Results have been presented from a series of calculations performed using the old (rather crude) representation of a hemispherical vessel. In particular the sensitivity of the mass of material mixed to parameters in the drag law has been studied and the results are found to be relatively insensitive for a large change in the drag coefficient and assumed (constant) water and steam length-scales. Further calculations to investigate the effect of melt and water fragmentation have also been performed. We have observed that allowing for melt and water break-up can lead to quite complicated effects. For example, as the melt fragments a considerable amount of steam is generated, which fragments the water, the water is swept-out and the mixing is limited. In a simulation where this feedback mechanism was not present the high heat transfer rate was sustained for longer and the pressure in the vessel rose by 5bars. These results illustrate the highly complex nature of the system being modelled.

4.1 Status of Model Validation

The CHYMES code has been in existence for two years. Over that period it has been used, tested and modified a number of times to improve its user-friendliness and robustness. Each run provides a diagnostic output which allows the user to ensure that the solution is stable and that a sufficiently small time-step has been used. Each subroutine has been thoroughly tested and the purpose of each subroutine is clearly defined.

The physical models in the code have been less well tested. A 1D version of the code was used to simulate a 1D experiment performed at Brookhaven National Laboratory [22], in which steel shot was dropped into saturated water. This results from this experiment consisted of the transient steaming rate and a few qualitative observations. These were successfully simulated, as reported in reference 7. A 2D experiment, using a jet of Corium poured into saturated water (experiment CWTI-9) was performed at Argonne National Laboratory [23]. The experimental data was in the form of the transient vessel pressurization, some sweep-out data, the final melt particle size distribution and qualitative information obtained using X-ray cine photography. Good agreement with this data was obtained (considering that a number of geometrical features of the experiment could not be modelled) and is reported in references 8 and 9. Due to the lack of quantitative data no other experimental simulations have been performed, although many qualitative features of experimental studies have been reproduced. For example, the effect of ambient pressure variation was reported in references 7 and 8 and the effect of melt composition was studied in reference 11. The sensitivity of the mixing process to the initial conditions has become evident from a number of simulations. In particular, the initial radial velocity of the jet has been illustrated to be important [11].

4.2 Future Work

The major developmental work is now completed. In the future the code will be made fully compressible so that vapour condensation in subcooled water can be modelled. In addition, the effect of vapour superheat will be examined. These changes are relatively easy to make.[2] This change will make the code more versatile and increase the range of problems for which it can be used but it will also increase the number of constitutive relations needed.

The main requirement of future work is experimental validation of the model and the constitutive relations employed in it. This can be carried out in a number of ways:

1. By performing small-scale experiments with simulant materials to validate the drag or heat transfer modelling. In principle these type of experiments would be very easy to perform but it must be remembered that in the real problem the high heat transfer rates produce very different flow conditions compared with heated shot dropped into water. In addition, any experiment which does not produce quantitative results for quantities, such as, sweep-out, level-swell, steaming rates etc. is of little use, since we already know that the code produces qualitatively correct results.

2. Well instrumented intermediate scale experiments, of the type performed at Argonne, would be very useful to further check the integrated model.

3. Specific features of the code could be enhanced using experimental data from, for example, Sandia National Laboratory or Argonne. In particular, results from the jet-mixing experiments currently being analysed at Sandia [24] and Argonne [25] could be used to implement a model of jet breakup. In this case close access to the experimental data is required. (The length-scale model would have to be modified to cope with situations where melt zones have a characteristic dimension greater than the finite difference cell size [14].)

4. Simulations presented in this paper have highlighted the possible importance of modelling mixing in stratified layers.

To summarise, the mathematical development of CHYMES is virtually completed but the experimental validation of the model is only just beginning. To make further use of CHYMES to determine what mixture can support a propagating detonation it will also be necessary to replace our qualitative understanding of what constitutes a good mixture by a quantitative one. To do this a detonation model, called CULDESAC, is currently under development [26,27,28,29]. In the future, results similar to those presented here will be used as part of a probabilistic study to determine a new estimate for the probability of alpha-mode failure [5].

[2]The main difficulty is in obtaining a suitable water equation of state for this purpose.

Acknowledgements

This work was funded by the General Nuclear Safety Research (GNSR) programme. The author would like to thank Dr. A. Thyagaraja for stimulating discussions during the course of this work and to thank Mr. I. Cook for useful comments on a draft of this paper.

References

[1] A.W. Cronenberg, *Recent developments in the understanding of energetic molten fuel coolant interaction.* Nucl. Safety, **21**, 319-337, (1980).

[2] T.G. Theofanous et al., *An assessment of steam-explosion-induced containment failure.* Nucl. Sci. Eng., **97**, 259-325, (1987).

[3] M. Berman, D.V. Swenson, and A.J. Wickett, *An uncertainty study of PWR steam explosions.* NUREG/CR-3369, (1984).

[4] SERG (Steam Explosion Review Group) *A review of the current understanding of the potential for containment failure arising from in-vessel steam explosions.* NUREG/CR-1116, (1985).

[5] I. Cook, *Assessment of large-scale, in-vessel, steam explosions.* In Nuclear safety after Three Mile Island and Chernobyl, edited by G.M. Ballard, Elsevier Applied Science, London, (1988).

[6] D.F. Fletcher, *A review of coarse mixing models.* Culham Laboratory Report: CLM-R251, (1985).

[7] D.F. Fletcher and A. Thyagaraja, *Numerical simulation of one-dimensional multiphase mixing.* Culham Laboratory Report: CLM-P776, (1986).

[8] A. Thyagaraja and D.F. Fletcher, *Buoyancy-driven, transient, two-dimensional thermo-hydrodynamics of a melt-water-steam mixture.* Comput. Fluids, **16**(1), 59-80, (1988).

[9] D.F. Fletcher and A. Thyagaraja, *Numerical simulation of two-dimensional transient multiphase mixing.* Proc. 5th Int. Conf. on Numerical Methods in Thermal Problems, Montreal, Canada, June 29th - July 3rd 1987, **V**(2), 945-956, Pineridge, (1987).

[10] D.F. Fletcher and A. Thyagaraja, *A method of quantitatively describing a multicomponent mixture.* PhysicoChem. Hydrodynam., 9(3/4), 621-631, (1987).

[11] D.F. Fletcher and A. Thyagaraja, *A mathematical model of premixing.* Paper to be presented at the 25th ASME/AIChE National Heat Transfer Conference, Houston, Texas, 24-27 July, 1988.

[12] D.F. Fletcher, *Large scale mixing calculations.* Culham Laboratory Report: CLM-R282, (1988).

[13] D.F. Fletcher and A. Thyagaraja, *A computer model of multiphase mixing.* Paper presented at the Polymodel XI Conference on Flow Modelling in Industrial Flow

Processes, Teesside, 24-25 May, 1988. (Proceedings to appear.)

[14] M.F. Young, *IFCI: an integrated code for calculation of all phases of fuel-coolant interactions.* NUREG/CR-5084, (1987).

[15] F.H. Harlow and A.A. Amsden, *Flow of interpenetrating material phases.* J. Comput. Phys., **18**, 440-465, (1975).

[16] D.F. Fletcher, *Assessment and development of the Bankoff and Han coarse mixing model.* Culham Laboratory Report: CLM-R252, (1985).

[17] L.C. Witte, *Film boiling from a sphere.* I & EC Fundamentals, **7**, 517-518, (1968).

[18] M.A. Abofadl and T.G. Theofanous, *An assessment of steam-explosion-induced containment failure. Part II: Premixing Limits.* Nucl. Sci. Engng., **97**, 282-295, (1987).

[19] D.F. Fletcher, *The particle size distribution of solidified melt debris from molten fuel-coolant interaction experiments.* Nucl. Engng. Des., **105**(3), 313-319, (1988).

[20] M.L. Corradini, A proposed model for fuel-coolant mixing. Trans. Am. Nucl. Soc., **41**, 415-416, (1982).

[21] J.J. Sienicki and B.W. Spencer, *Analysis of reactor material experiments on corium-water thermal interactions in ex-vessel geometry.* Proc. Int. Meeting on light water reactor severe accident evaluation, Cambridge, Massachusetts, August 28 - September 1, (1983).

[22] G.A. Greene, T. Ginsberg and N.K. Tut, *BNL severe accident sequence experiments and analysis program.* Proc. 12th NRC water reactor information meeting, Gaitisburg, USA, **3**, (1885).

[23] B.W. Spencer, L. Mcumber, D. Gregorash, R. Aeschlimann and J.J. Sienicki, *Corium quench in deep pool mixing experiments.* Proc. National Heat Transfer Conf., Denver, Colorado, USA, August, (1985).

[24] B.W. Marshall, *Jet mixing experiments.* In Reactor Safety Research Semiannual Report July-December, 1986, **36**, NUREG/CR-4805, (1987).

[25] B.W. Spencer, J.D. Gabor and J.C. Cassulo, *Effect of boiling regime on melt stream breakup in water.* Proc. 4th Miami Int. Symp. on Multi-phase Transport and Particulate Phenomena, Miami Beach, Florida, 15-17 December, 1986.

[26] D.F. Fletcher and A. Thyagaraja, *Some calculations of shocks and detonations for gas mixtures.* Culham Laboratory Report: CLM-R276, (1987). (To appear in Computers and Fluids.)

[27] D.F. Fletcher and A. Thyagaraja, *Multiphase flow simulations of shocks and detonations, Part I: Mathematical formulation and shocks.* Culham Laboratory Report: CLM-R279, (1987).

[28] A. Thyagaraja and D.F. Fletcher, *Multiphase flow simulations of shocks and detonations, Part II: Detonations.* Culham Laboratory Report: CLM-R280, (1987).

[29] D.F. Fletcher and A. Thyagaraja, *Multiphase flow simulations of shocks and detonations, Part III: Droplet laden gas flows.* Culham Laboratory Report: CLM-R283, (1988).

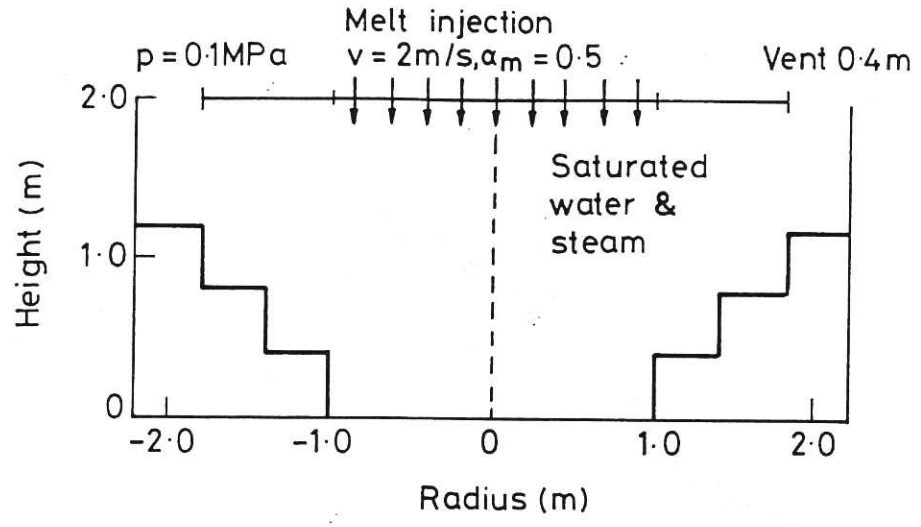

(a) Old geometry.

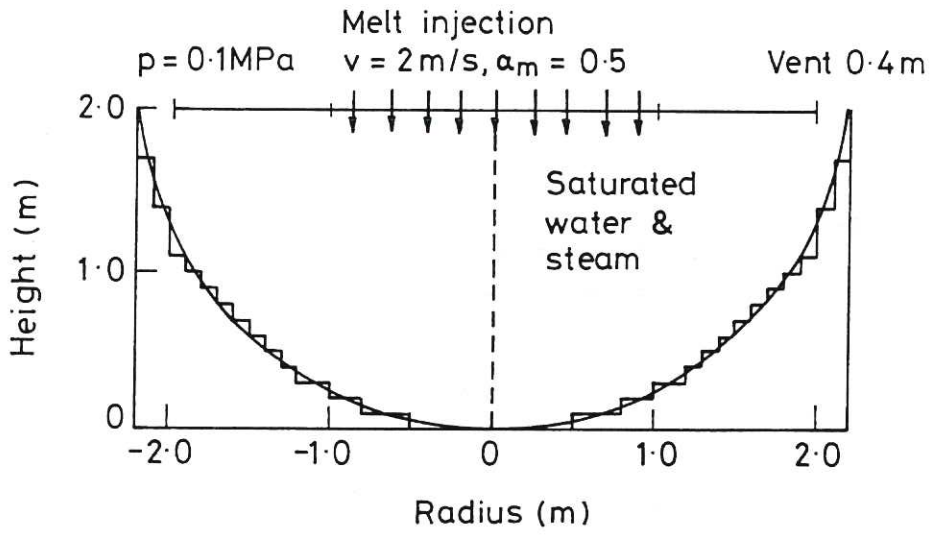

(b) New geometry.

Fig. 1 Geometry used in the simulations.

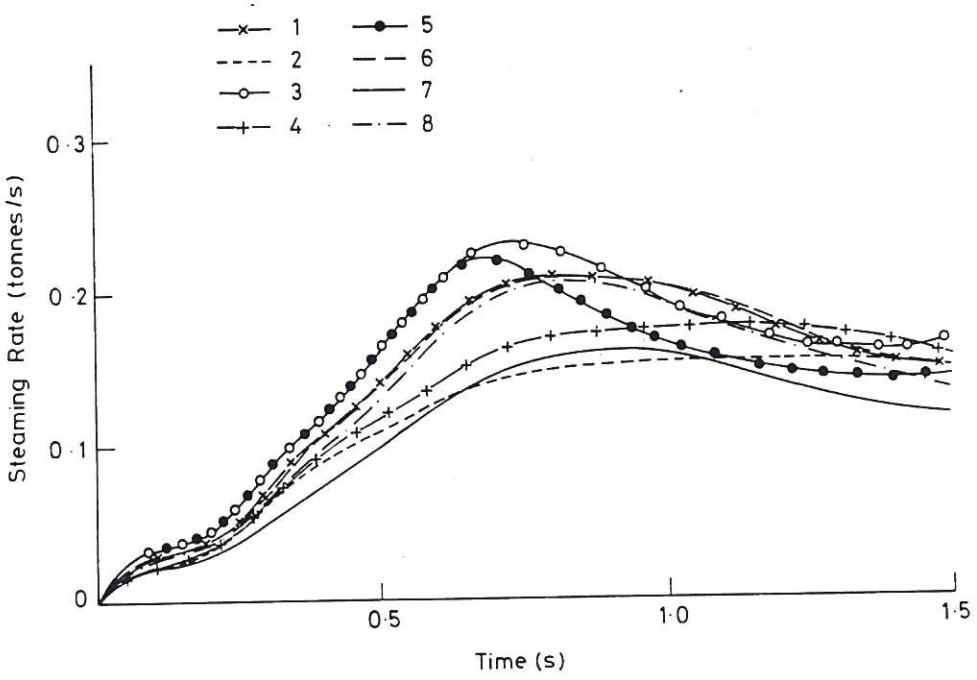

Fig. 2 The transient steaming rate.

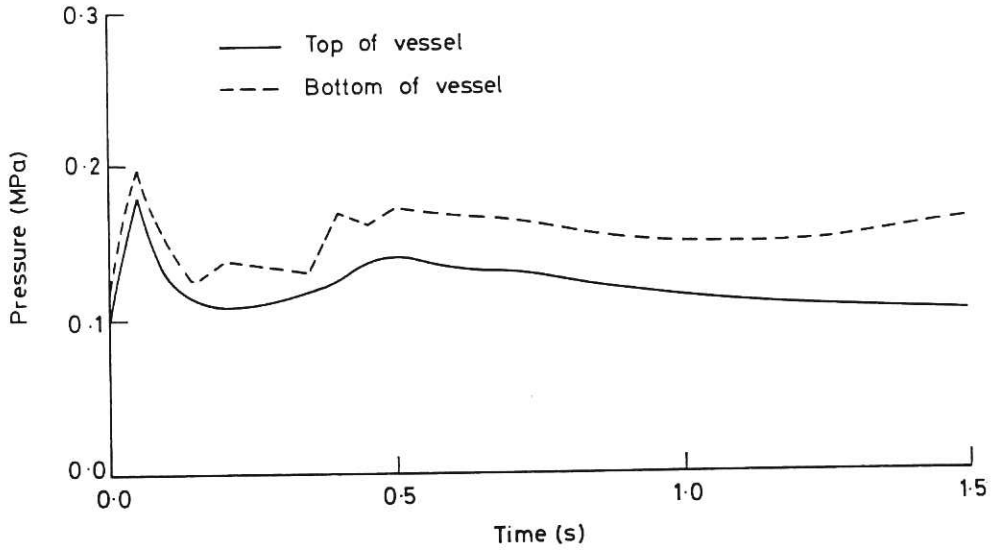

Fig. 3 Pressure on the axis of the vessel for the Base Case Calculation.

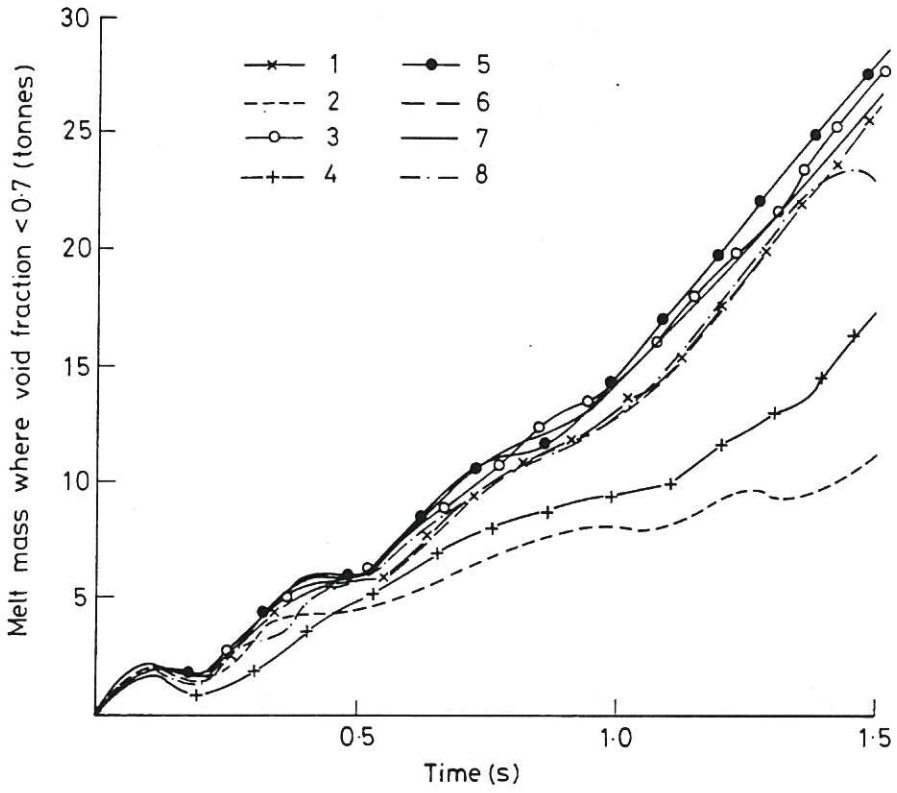

Fig. 4 Mass of melt where void fraction <0.7 as a function of time.

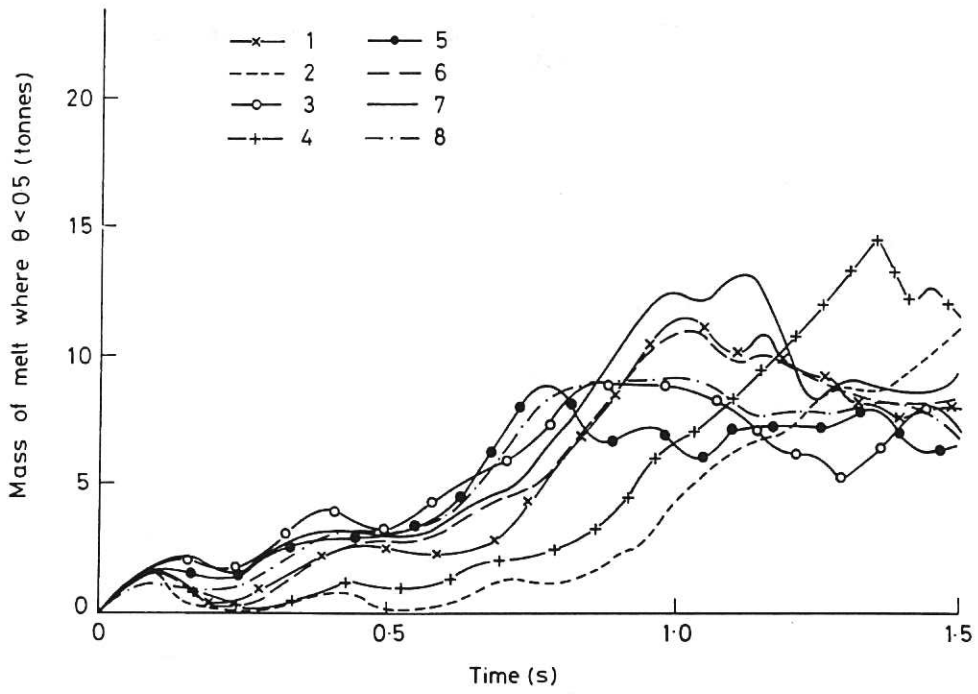

Fig. 5 Mass of melt where $\theta<0.5$ as a function of time.

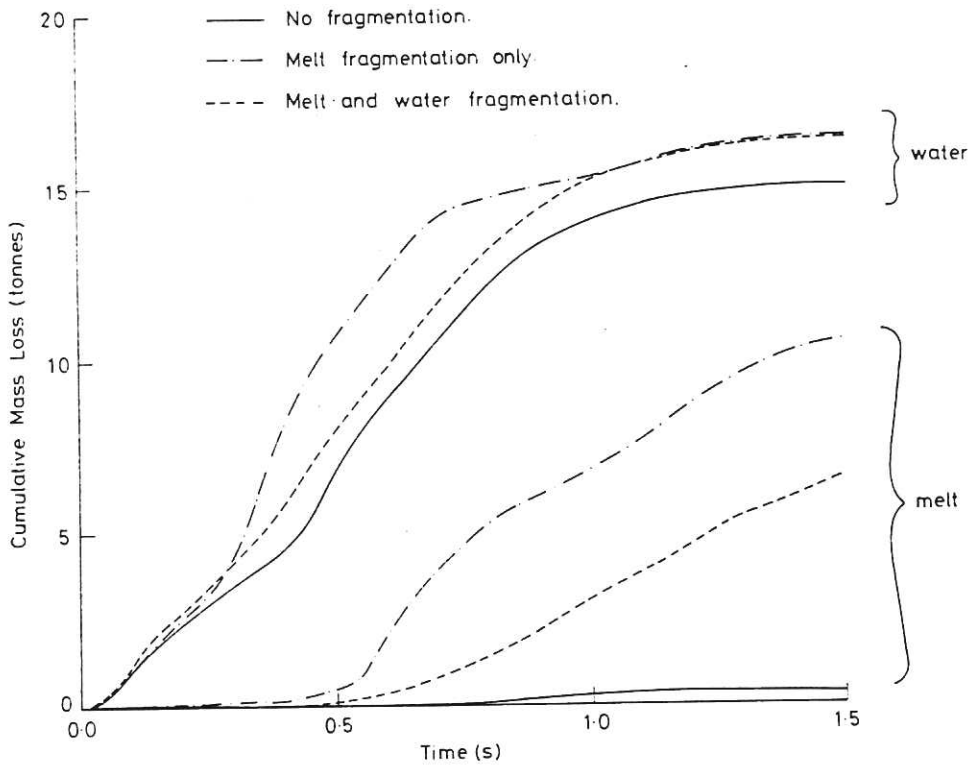

Fig. 6 Transient sweep-out of melt and water.

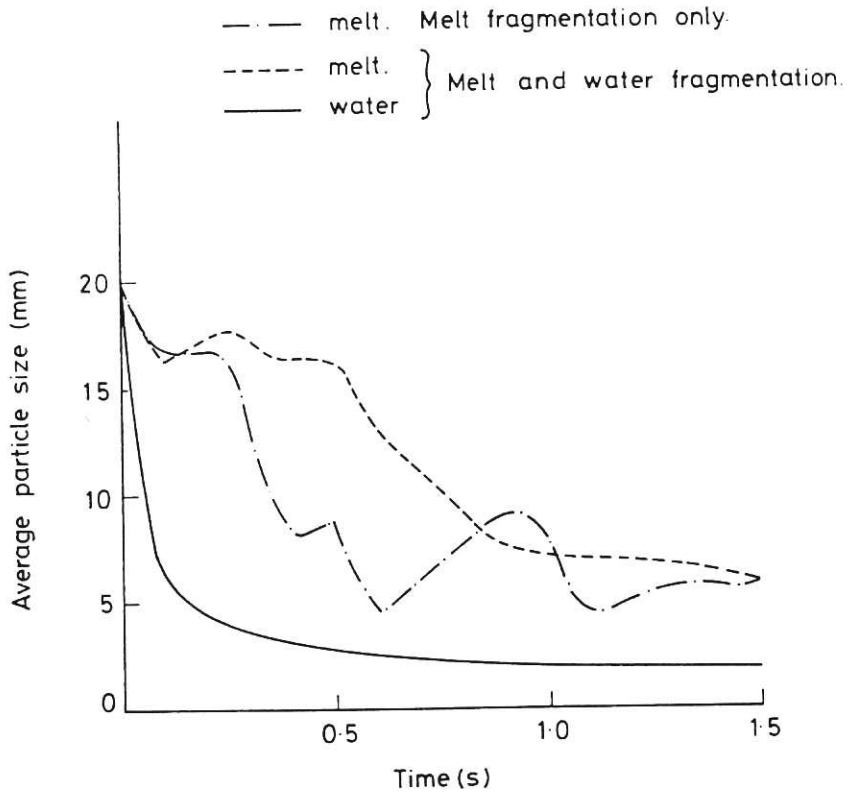

Fig. 7 Average particle size as a function of time.

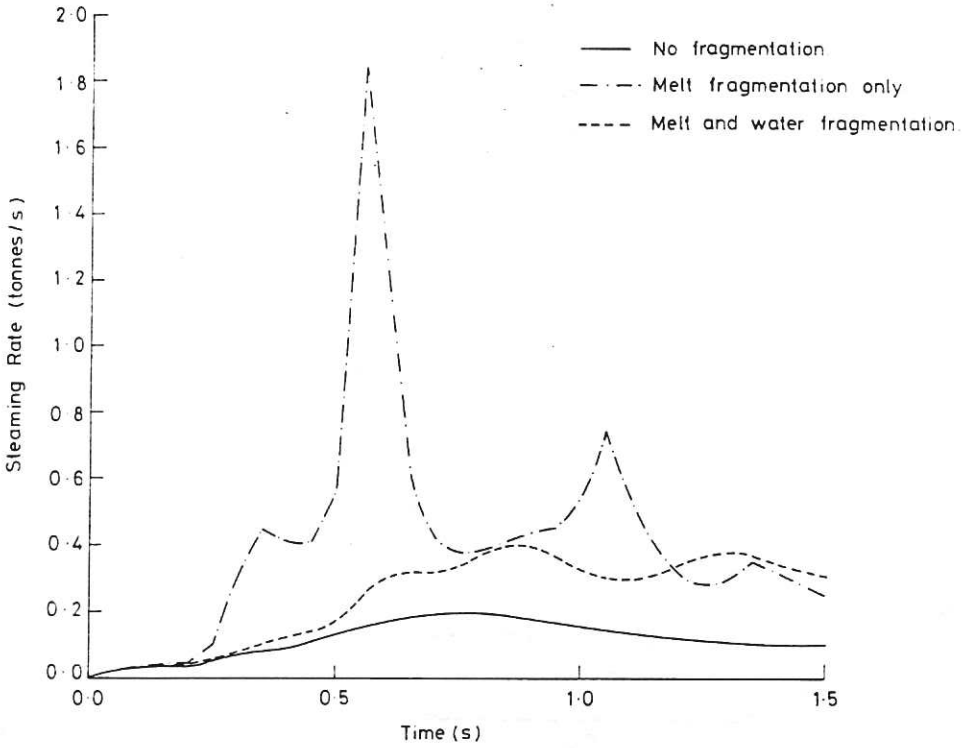

Fig. 8 The transient steaming rate.

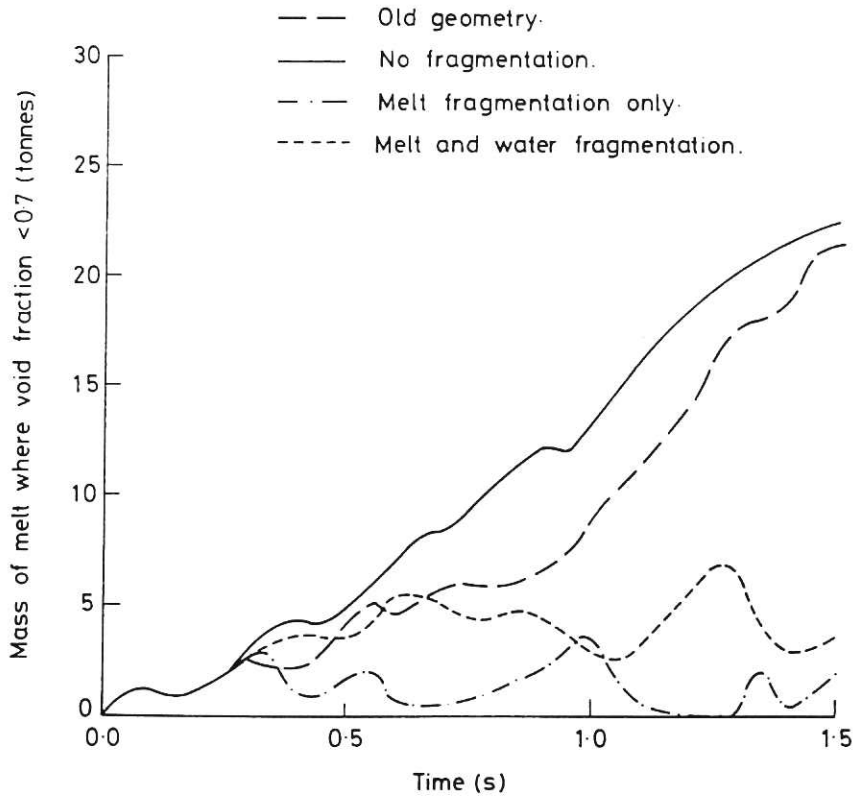

Fig. 9 Mass of melt where void fraction <0.7 as a function of time.

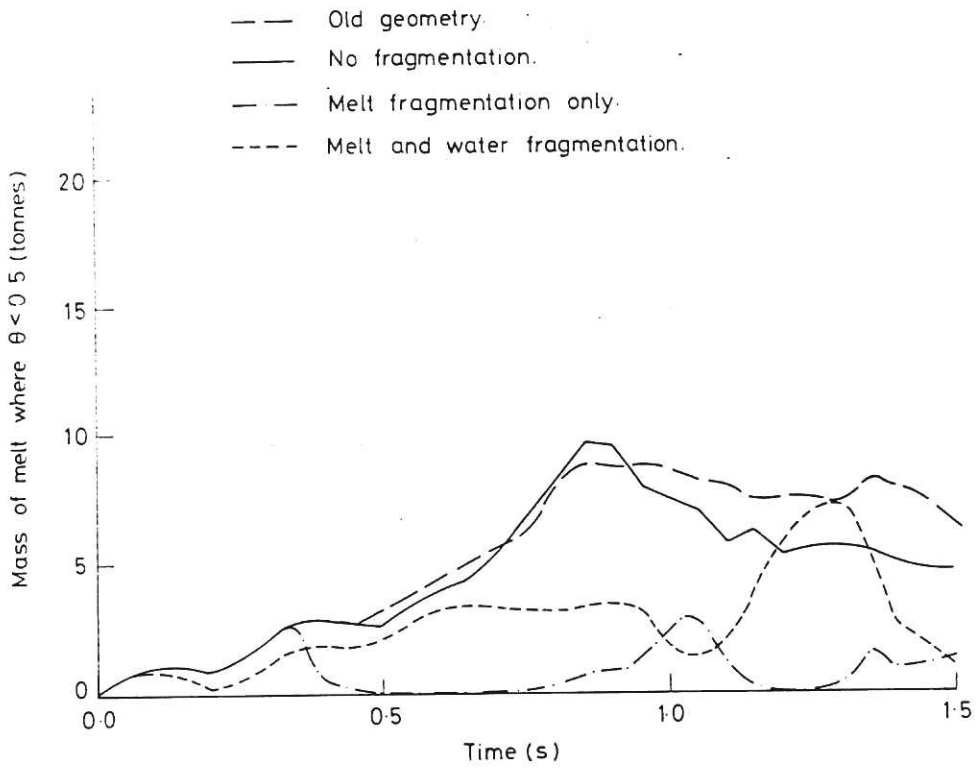

Fig. 10 Mass of melt where $\theta < 0.5$ as a function of time.

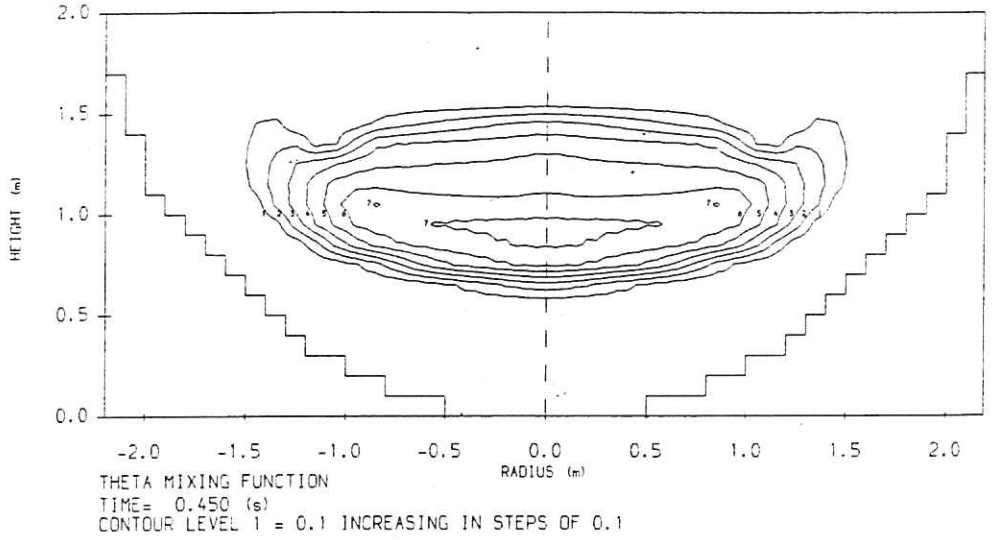

Fig. 11(a) Theta contours for Calc.9 at t=0.45s.

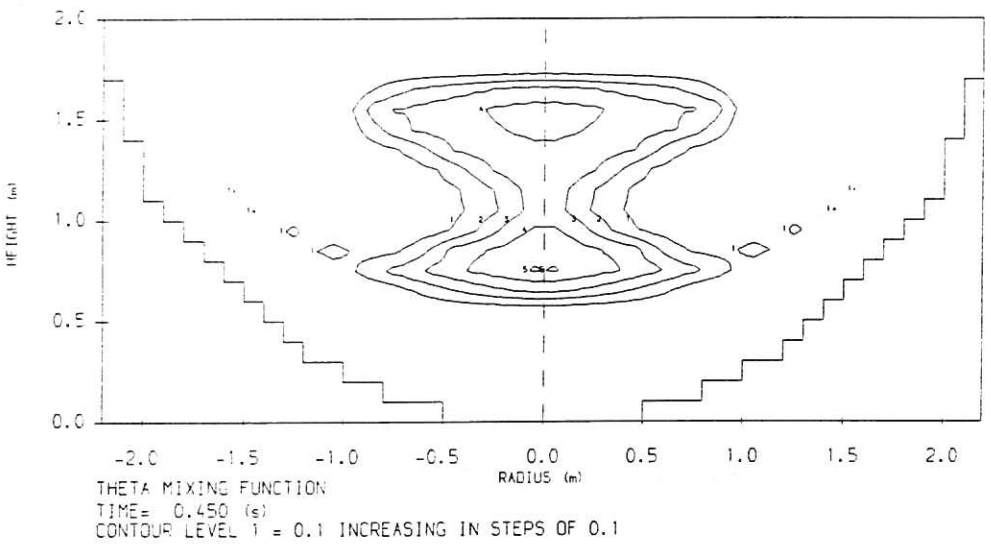

Fig. 11(b): Theta contours for Calc.10 at t=0.45s.

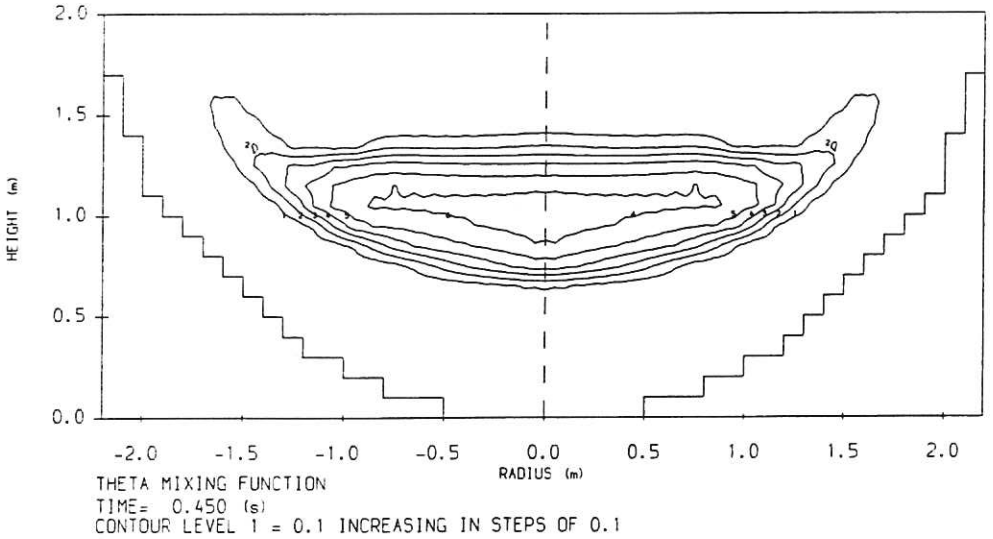

Fig. 11(c): Theta contours for Calc.11 at t=0.45s.

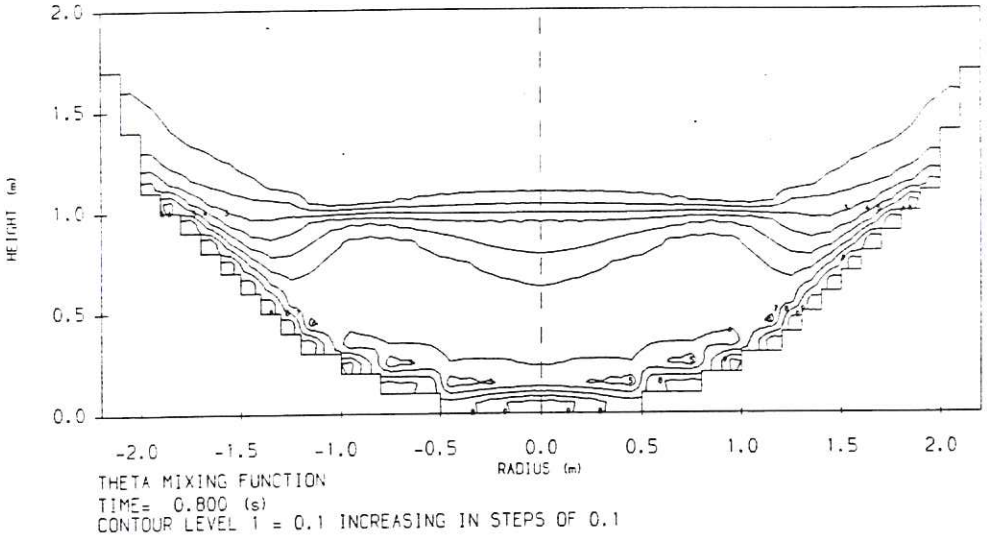

Fig. 12(a): Theta contours for Calc.9 at t=0.8s.

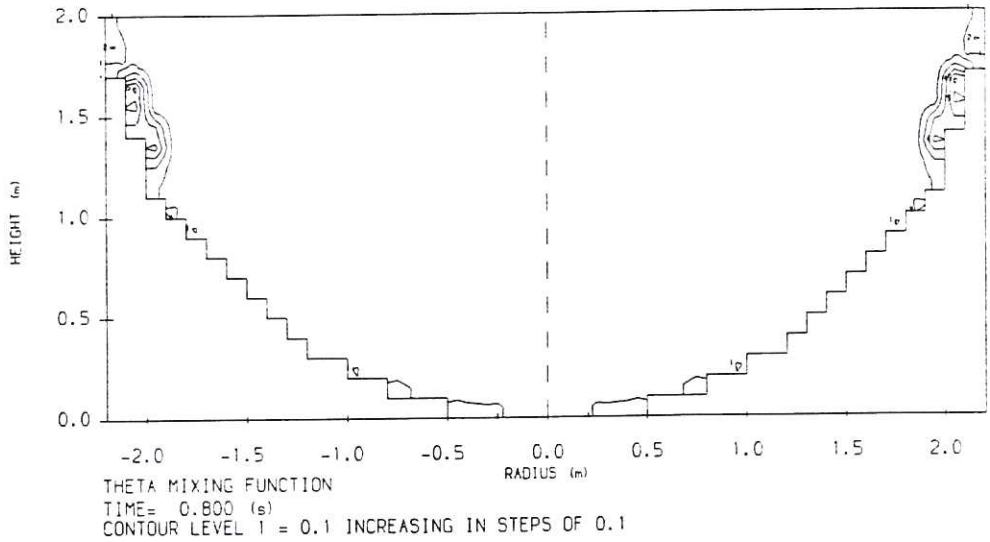

Fig. 12(b): Theta contours for Calc.10 at t=0.8s.

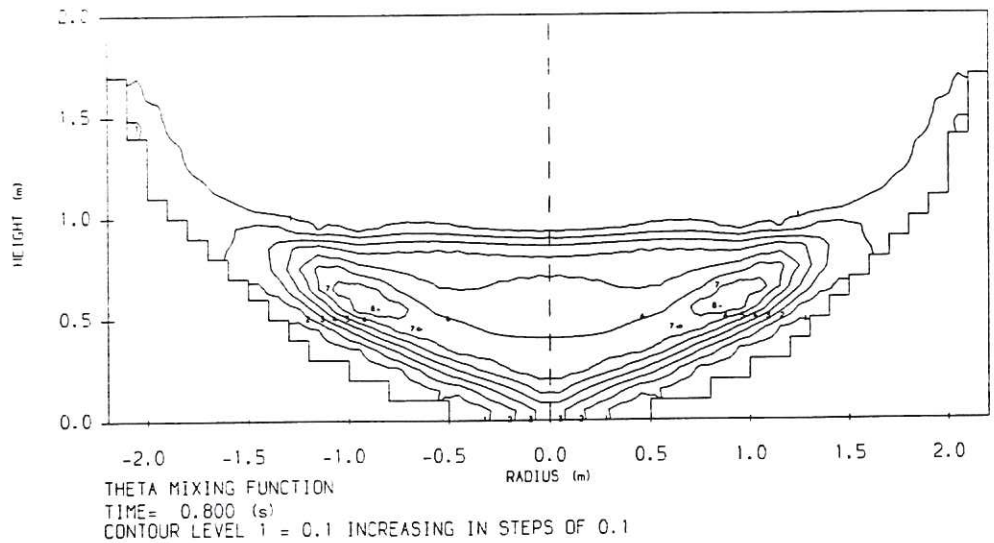

Fig. 12(c): Theta contours for Calc.11 at t=0.8s.

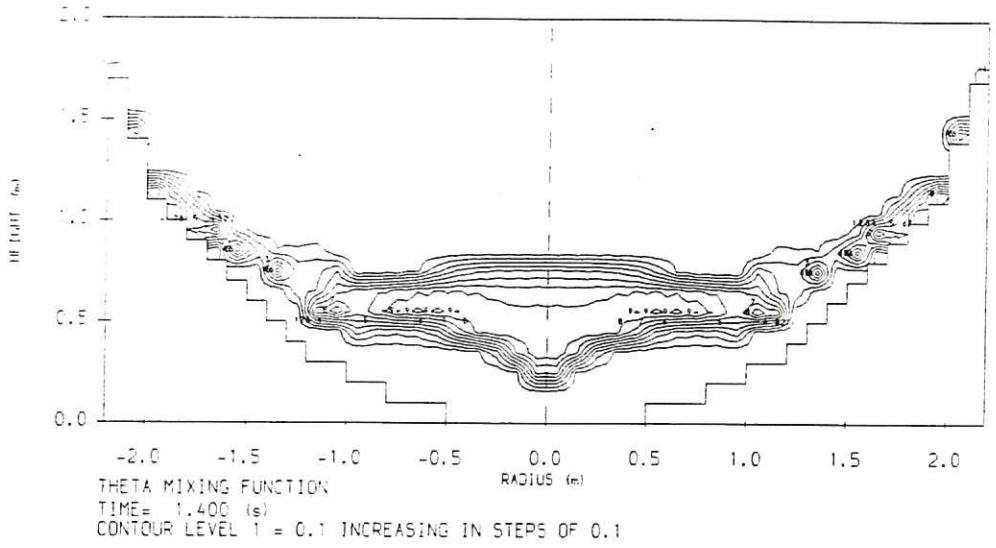

Fig. 13(a): Theta contours for Calc.9 at t=1.4s.

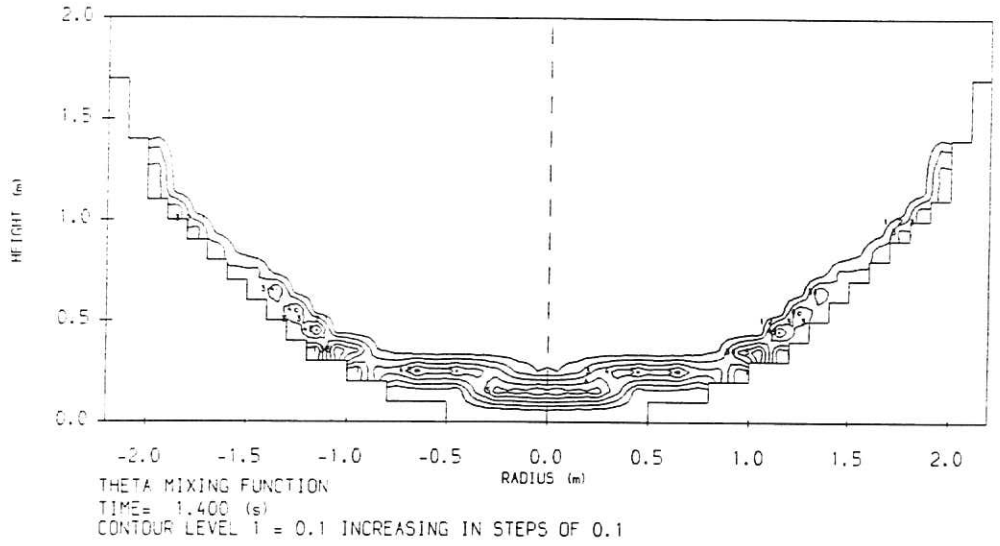

Fig. 13(b): Theta contours for Calc.10 at t=1.4s.

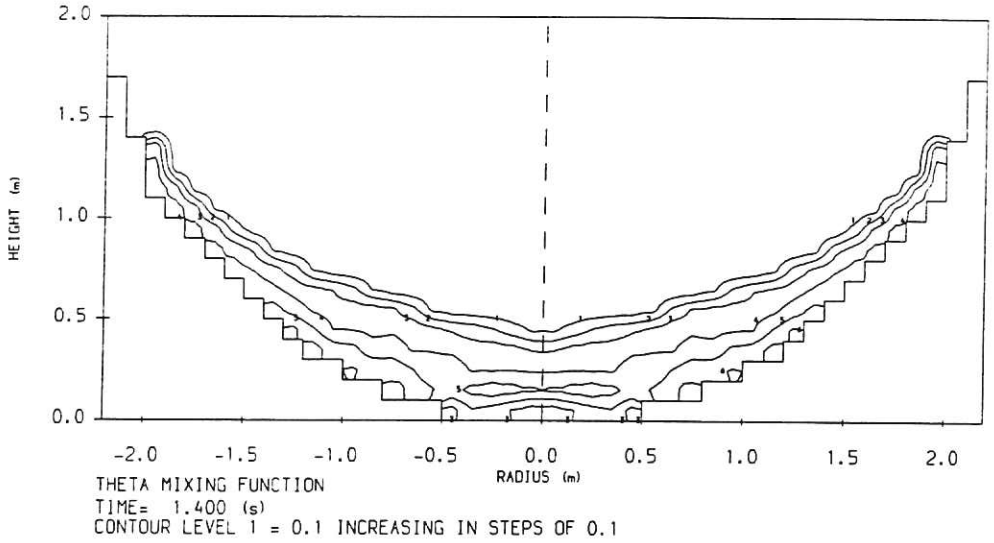

Fig. 13(c): Theta contours for Calc.11 at t=1.4s.